computation

Article

Multiscale Simulations for Coupled Flow and Transport Using the Generalized Multiscale Finite Element Method

Eric T. Chung [1]**, Yalchin Efendiev** [2,3,]*****, Wing Tat Leung** [3] **and Jun Ren** [3]

[1] Department of Mathematics, The Chinese University of Hong Kong, Shatin, Hong Kong, China;
   E-Mail: eric.t.chung@gmail.com

[2] Center for Numerical Porous Media (NumPor), King Abdullah University of Science and Technology
   (KAUST), Thuwal 23955-6900, Saudi Arabia

[3] Department of Mathematics, Texas A&M University, College Station, TX 77843, USA;
   E-Mails: sidnet123@gmail.com (W.T.L.); ustcrenjun@gmail.com (J.R.)

***** Author to whom correspondence should be addressed; E-Mail: efendiev@math.tamu.edu;
   Tel.: +1-979-485-0098.

Academic Editors: Qinjun Kang and Li Chen

Abstract: In this paper, we develop a mass conservative multiscale method for coupled flow and transport in heterogeneous porous media. We consider a coupled system consisting of a convection-dominated transport equation and a flow equation. We construct a coarse grid solver based on the Generalized Multiscale Finite Element Method (GMsFEM) for a coupled system. In particular, multiscale basis functions are constructed based on some snapshot spaces for the pressure and the concentration equations and some local spectral decompositions in the snapshot spaces. The resulting approach uses a few multiscale basis functions in each coarse block (for both the pressure and the concentration) to solve the coupled system. We use the mixed framework, which allows mass conservation. Our main contributions are: (1) the development of a mass conservative GMsFEM for the coupled flow and transport; (2) the development of a robust multiscale method for convection-dominated transport problems by choosing appropriate test and trial spaces within Petrov-Galerkin mixed formulation. We present numerical results and consider several heterogeneous permeability fields. Our numerical results show that with only a few basis functions per coarse block, we can achieve a good approximation.

---

1. Introduction

Many porous media problems occur over multiple scales. Because of scale disparity, some type of model reduction or averaging are often employed. Typical flow-based upscaling approaches ([1–3]) compute the permeabilities on a coarse (computational) grid and solve the flow and transport equations together on a coarse grid. These approaches are easy to implement with a minimal code modification; however, these approaches can result in large errors for complex heterogeneities because limited information is used in upscaling. In this paper, we consider a multiscale method for a coupled flow and transport system, where the flow equation for the pressure field is described by a steady state elliptic equation (derived by Darcy law) and the transport equation for the concentration field is described by a convection-dominated parabolic equation.

Our approach derives its foundation from rigorous multiscale techniques developed recently [4–25]. In our approach, multiscale basis functions are computed and used to solve flow equations. The main contributions of this paper are (1) to use multiscale basis functions for both flow and transport equations and (2) design of a novel mixed multiscale methods for convection-dominated transport equations within the context of Generalized Multiscale Finite Element Method (GMsFEM). The GMsFEM is introduced in [16], where the objective is to construct multiscale basis functions in each coarse domain. The main distinction of this approach from some of existing multiscale methods is that the GMsFEM systematically constructs multiscale basis functions using local spectral problems and the local snapshot spaces. Both of these concepts (local spectral problem and local snapshot spaces) are important in a design of the method.

In our proposed approach, we use a mixed formulation for both the flow and the transport equations. The use of a mixed formulation for the flow equation guarantees the mass conservation [7,26–30]. The use of a mixed formulation is important for the transport equation, guarantees the mass conservation and helps with the stabilization of it. In particular, by adding more flux basis functions, we can achieve a better stability based on our numerical studies [31]. In the mixed formulation for a coupled system, we first define snapshot spaces for the appropriately defined fluxes in the flow and the concentration equations. For the pressure and the concentration fields, we use piecewise constant basis functions. The snapshot space represents the solution space in each coarse region and provides a mass conservative approach. In the snapshot space, we perform a local spectral decomposition to identify multiscale basis functions. The functions corresponding to dominant modes are used to construct coarse spaces for the fluxes. In particular, we use only a few degrees of freedom (maximum two) in each coarse region. For the test functions for the convection-dominated transport, we use the solutions of adjoint problem. As a result, we have a full coarse-grid approximation for the coupled flow and transport system.

We would like to discuss a relation between our proposed approaches and the flow-based upscaling [2,3]. In the latter, the upscaled permeabilities are computed and, then, the coupled flow and transport equation is solved on a coarse grid. The computations of upscaled permeabilities can be compared to the computations of multiscale basis functions, which are performed locally in each

coarse region by solving local problems. The resulting coarse-grid problem in the upscaled model is similar to our resulting coarse-grid system. There are several main advantages of the proposed method: (1) it can use more multiscale basis functions in each region and achieve a desired accuracy; (2) the number of multiscale basis functions can be adaptively selected in space and time; (3) our approach can easily reconstruct the fine-scale distributions of the solution; (4) our approaches can handle any coarse-grid geometries.

We consider several numerical examples by considering two different hydraulic conductivity fields. In our numerical examples, we use a relatively coarse grid with the coarsening factor of 20. We study the numerical errors in the concentration field and depict concentration profiles at different time instants. Our numerical results show that the use of only one basis function per coarse edge (which is similar to numerical upscaling of hydraulic conductivity) does not produce an accurate solution, while if we use two basis functions, we can obtain a much more accurate approximation of the solution. These preliminary numerical results show that our fully coarse-grid model for the coupled flow and transport equations can accurately predict the solution using only a few degrees of freedom in each coarse region.

Novelty. The novelty of our work can be summarized as follows:

- The development of Generalized Multiscale Finite Element Method for a mixed formulation of the convection-diffusion equation using different test and trial spaces.

- The development and implementation of a mass conservative mixed GMsFEM for the coupled flow and transport equations.

The paper is organized as follows. In the next section, we present preliminaries and describe coarse and fine grids as well as a mixed formulation. Section 3 is devoted to the construction of multiscale basis functions. Numerical results are presented in Section 4. Finally, we present conclusions.

2. Preliminaries and Notations

We consider a coupled flow and transport system that arises in many hydrological applications

$$
\begin{aligned}
\frac{\partial c}{\partial t} + v \cdot \nabla c - D\Delta c &= f_c && \text{in } \Omega \times (0, T), \\
v + \kappa \nabla p &= 0 && \text{in } \Omega, \\
\nabla \cdot v &= f_q && \text{in } \Omega.
\end{aligned}
\tag{1}
$$

Here Ω is the computational domain, $T > 0$ is a fixed time, κ is a hydraulic conductivity, c is the concentration, p is the pressure, D is a diffusivity of the medium, and f_c, f_q are source terms. The equations are subject to the boundary conditions $c(x, t) = 0$ on $\partial\Omega \times [0, T]$, $p(x) = g$ on $\partial\Omega$ and the initial condition $c(x, 0) = 0$ in Ω. In order to have a mass conservation, we re-write the system in a mixed formulation.

$$
\begin{aligned}
\frac{\partial c}{\partial t} + \nabla \cdot q &= f_c + cf_q && \text{in } \Omega \times (0, T), \\
q + D\nabla c - vc &= 0 && \text{in } \Omega \times (0, T), \\
v + \kappa \nabla p &= 0 && \text{in } \Omega, \\
\nabla \cdot v &= f_q && \text{in } \Omega.
\end{aligned}
\tag{2}
$$

Here q is an auxiliary variable, we call it flux or flux-concentration. It is well known that the Galerkin method inherits the stability of the continuous problem, and it yields to spurious oscillation when the convection coefficient is larger than the diffusive one ($v \gg D$). The mixed finite element methods can be used to achieve a mass conservation. In this paper, we aim to construct multiscale basis functions for the flux q and the velocity v. As for the concentration c and the pressure p, we choose piecewise constant functions on a coarse grid.

Next, we introduce the discretized form of the Problem (2). We first comment on some notations of the coarse and the fine mesh. We assume that Ω is partitioned in a usual way into a union of rectangles (in 2-D) or hexadedrals (in 3-D) denoted by $\mathcal{T}^H$, where H is the coarse mesh size. The fine mesh is obtained by splitting each coarse block in $\mathcal{T}^H$ into a connected union of fine-grid blocks, and we denote it by $\mathcal{T}^h$ with mesh size h, $h < H$. In addition, we denote by $\mathcal{E}^H$ the set of all edges/faces of elements in $\mathcal{T}^H$, *i.e.*, $\mathcal{E}^H = \{E_i : 1 \leq i \leq N_e\}$, where N_e is the number of coarse edges/faces. Note that each $E_i \in \mathcal{E}^H$ is the union of some fine-grid edges/faces. That is, $E_i = \{e_j : e_j \text{ is on } E_i\}$, where e_j are the fine-grid edges/faces lying on E_i. We also define the coarse neighborhood of the edge/face E_i by

$$\omega_i = \{K \in \mathcal{T}^H : \partial K \cap E_i \neq \phi\}. \tag{3}$$

See Figure 1 for an illustration of a coarse neighborhood associated with one coarse edge, where the coarse mesh and the fine mesh are represented by black lines and gray lines, respectively.
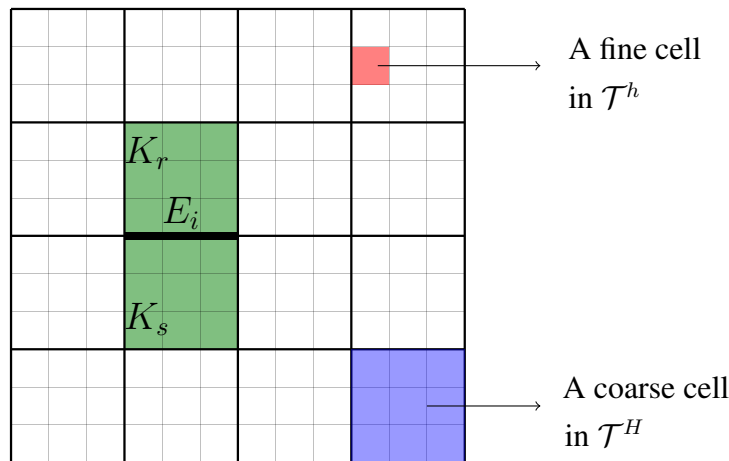
Figure 1. An illustration of a coarse neighborhood ω_i (in green) corresponding to the coarse edge E_i.

Next, we define the coarse trial spaces for q, v, c, and p. The concentration c and the pressure p are approximated in the space of piecewise constant functions with respect to the coarse grid $\mathcal{T}^H$. We denote this space by Q_H, and

$$Q_H = \{\psi : \psi|_{K_i} \in \mathcal{P}_0(K_i) \text{ for all } K_i \in \mathcal{T}^H\}. \tag{4}$$

As for the flux-concentration q and the velocity v, the basis functions are associated with coarse edges and are supported in the corresponding coarse neighborhoods. In particular, to obtain the basis functions for a coarse edge E_i, we will solve a local problem in the coarse neighborhood ω_i. Let Φ_i^q and Φ_i^v be

the set of multiscale basis functions for q and v with respect to E_i, respectively. Then, we define the multiscale solution space for q and v as

$$V_H^q = \bigcup_{E_i} \Phi_i^q \quad \text{and} \quad V_H^v = \bigcup_{E_i} \Phi_i^v. \tag{5}$$

Furthermore, we discretize the time interval $[0, T]$ uniformly by the points

$$t^n = n\tau, \quad n = 0, 1, \cdots, N$$

where τ is the time step and $N = T/\tau$. Using the above spaces, the GMsFEM approximation of (2) can be given as follows. For all $n \geq 1$, find $(c_H^n, q_H^n, p_H, v_H) \in Q_H \times V_H^q \times Q_H \times V_H^v$, such that

$$
\begin{aligned}
\int_\Omega \frac{c_H^n - c_H^{n-1}}{\tau} \tilde{c} + \int_\Omega (\nabla \cdot q_H^{n-\theta}) \tilde{c} &= \int_\Omega (f_c^{n-\theta} + c_H^{n-\theta} f_q) \tilde{c} && \text{for } \forall \tilde{c} \in Q_H, \\
\int_\Omega \frac{1}{D} q_H^{n-\theta} \cdot \tilde{q} &= \int_\Omega (\nabla \cdot \tilde{q} + \frac{v_H}{D} \cdot \tilde{q}) c_H^{n-\theta} && \text{for } \forall \tilde{q} \in W_H^q, \\
\int_\Omega \frac{1}{\kappa} v_H \cdot \tilde{v} &= \int_\Omega (\nabla \cdot \tilde{v}) p_H && \text{for } \forall \tilde{v} \in V_H^v, \\
\int_\Omega (\nabla \cdot v_H) \tilde{p} &= \int_\Omega f_q \tilde{p} && \text{for } \forall \tilde{p} \in Q_H,
\end{aligned} \tag{6}
$$

subject to the boundary condition $p_H = g$. Here, we let $z^{n-\theta} = \theta z^{n-1} + (1 - \theta) z^n$, where $z = c_H$ or q_H. For $\theta = 0, 1/2$ and 1, we get the Backward Euler, Crank-Nicolson and Forward Euler Methods respectively. Note that W_H^q is the testing space for q_H^n. We emphasize that in general, $W_H^q \neq V_H^q$, which allows a better stability. The construction of V_H^q, V_H^v, and W_H^q will be discussed in the next section.

In addition, to get the fine-scale solution, we use the standard lowest-order Raviart-Thomas space $Q_h \times V_h^q \times Q_h \times V_h^v$ for the approximation of (2) on the fine grid $\mathcal{T}^h$. The fine-scale solution (c_h, q_h) will be considered as a reference solution for the comparison with the multiscale solution (c_H, q_H).

3. Generalized Multiscale Finite Element Method

In this section, we will discuss the construction of the vector solution spaces V_H^q, V_H^v, and the testing space W_H^q. Note that solving q_H in (6) requires v_H. Therefore, we will first compute v_H using the last two equations of (6).

We briefly introduce the basic idea of the GMsFEM. In the framework of GMsFEM, it follows an offline-online procedure to generate the multiscale solution space. At the offline stage, we first construct the snapshot space obtained by solutions of local problems with all possible boundary conditions, which are resolvable by the fine-grid. Then, we choose a subspace of the snapshot space by selecting dominant modes via some local spectral decompositions. The resulting reduced dimensional space, called the offline space, will be used at the online stage to get a multiscale solution. Note that the snapshot space can be taken as the solution space to obtain a solution with a good accuracy. However, it is expensive to use the snapshot space due to its high dimensionality. Thus, there is a need to perform a space reduction within the snapshot space, and choose only few dominant modes to form the offline space. We remark that for parameter dependent problems (in which the coefficients depend on some extra parameters), one needs to construct an online space using the offline space and an appropriate spectral problem.

3.1. Multiscale Solution Space V_H^v

We form the multiscale solution space V_H^v for v_H. In order to build V_H^v, we first construct the snapshot space, denoted by V_{snap}^v. For each coarse-grid edge $E_i \in \mathcal{E}^H$, a local problem is defined on each of its neighboring coarse cells. Because the snapshot space is supposed to capture the multiscale information within this local domain, the corresponding boundary conditions of the local problem should cover all possibilities. Formally, the local problem is defined as the following: For each $E_i \in \mathcal{E}^H$, on its neighboring coarse cell $K = K_r$ or K_s (see Figure 2), find $(p_j^i, \psi_{v,j}^i) \in Q_h \times V_h^v$, such that

$$
\begin{aligned}
\psi_{v,j}^i + \kappa \nabla p_j^i &= 0 && \text{in } K, \\
\nabla \cdot \psi_{v,j}^i &= \alpha_j^i && \text{in } K, \\
\psi_{v,j}^i \cdot n &= 0 && \text{on } \partial K \backslash E_i, \\
\psi_{v,j}^i \cdot n &= \delta_j^i && \text{on } E_i.
\end{aligned}
\tag{7}
$$

Here, j varies over all fine-grid edges on E_i. For the convenience, we use the same notations as the solution to denote local snapshot fields. Here α_j^i is a constant defined on K, n is a fixed unit-normal vector on ∂K, and $\delta_j^i(x)$ is defined on E_i with respect to the fine-grid edges. Note that $E_i = \{e_j^i : e_j^i \text{ in } E_i\}$. We require δ_j^i has value 1 on e_j^i and 0 on the other fine-grid edges, $1 \leq j \leq J_i$, where J_i is the number of the fine-grid edges on E_i. That is,

$$
\delta_j^i = \begin{cases} 1, & \text{on } e_j^i, \\ 0, & \text{on the other fine-grid edges.} \end{cases}
$$
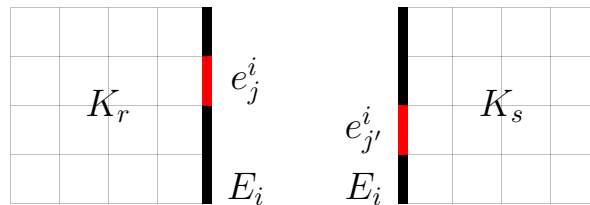
Figure 2. Neighboring coarse cells K_r and K_s corresponding to the coarse-grid edge E_i. The fine-grid edge e_j^i and $e_{j'}^i$ are in red.

Note that the constant α_j^i in (7) is chosen so that the compatibility condition $\int_K \alpha_j^i = (\pm) \int_{E_i} \delta_j^i$ is satisfied, for $K = K_r$ or K_s. The above local Problem (7) can be solved numerically on the underlying fine grid of K by the lowest-order Raviart-Thomas element method.

After solving the local problems (on K_r and K_s) with respect to E_i, a local snapshot $V_{\text{snap}}^{v,i}$ is generated by the solutions of (7). That is

$$
V_{\text{snap}}^{v,i} = \text{span}\{\psi_{v,j}^i : 1 \leq j \leq J_i\}.
$$

Then, the snapshot space V_{snap}^v is formed as

$$
V_{\text{snap}}^v = \bigcup_{E_i} V_{\text{snap}}^{v,i} = \text{span}\{\psi_{v,j}^i : 1 \leq j \leq J_i, 1 \leq i \leq N_e\}.
\tag{8}
$$

We re-numerate the snapshot functions by a single index to create the snapshot matrix

$$R_{\text{snap}}^v = \left[\psi_1^v, \psi_2^v, \cdots, \psi_{L_{\text{snap}}}^v \right],$$

where $L_{\text{snap}} = \sum_{i=1}^{N_e} J_i$ is the dimension of the snapshot space V_{snap}^v. Note that the matrix R_{snap}^v maps from the coarse space V_{snap}^v to the fine space. The next step is to construct the offline space V_{off}^v for v_H. For a coarse-grid edge E_i, we define the following eigenvalue problem in $V_{\text{snap}}^{v,i}$:

$$A_v^{\text{off}} \Psi_k^v = \lambda_k M_v^{\text{off}} \Psi_k^v, \tag{9}$$

where

$$A_v^{\text{off}} = [a_{st}] = \int_{E_i} (\psi_{v,s}^i \cdot n)(\psi_{v,t}^i \cdot n),$$

and

$$M_v^{\text{off}} = [m_{st}] = \int_{\omega_i} \frac{1}{\kappa} \psi_{v,s}^i \cdot \psi_{v,t}^i.$$

The eigenvalue Problem (9) will produce a set of eigenvectors for generating the local offline space $V_{\text{off}}^{v,i}$ by first selecting L_{off}^i eigenvectors corresponding to the smallest L_{off}^i eigenvalues, and then computing the element $\phi_{v,k}^i = \sum_{j=1}^{J_i} \Psi_{kj}^v \psi_{v,j}^i$ for $k = 1, 2, \cdots, L_{\text{off}}^i$, where Ψ_{kj}^v is the j-th component of Ψ_k^v. Then, the local offline space with respect to E_i is formed as

$$V_{\text{off}}^{v,i} = \text{span}\{\phi_{v,k}^i : 1 \le k \le L_{\text{off}}^i\}$$

and the offline space V_{off}^v is formed as

$$V_{\text{off}}^v = \bigcup_{E_i} V_{\text{off}}^{v,i} = \text{span}\{\phi_{v,k}^i : 1 \le k \le L_{\text{off}}^i, \ 1 \le i \le N_e\}. \tag{10}$$

We re-numerate the basis functions by a single index to create the offline matrix

$$R_{\text{off}}^v = \left[\phi_1^v, \phi_2^v, \cdots, \phi_{L_{\text{off}}}^v \right],$$

where $L_{\text{off}} = \sum_{i=1}^{N_e} L_{\text{off}}^i$ is the dimension of the offline space V_{off}^v.

We take the multiscale solution space as

$$V_H^v = V_{\text{off}}^v.$$

Then, v_H is approximated by solving the problem: Find $(p_H, v_H) \in Q_H \times V_H^v$ such that

$$\begin{aligned}
\int_\Omega \frac{1}{\kappa} v_H \cdot \tilde{v} &= \int_\Omega (\nabla \cdot \tilde{v}) p_H && \text{for } \forall \tilde{v} \in V_H^v, \\
\int_\Omega (\nabla \cdot v_H) \tilde{q} &= \int_\Omega f_q \tilde{q} && \text{for } \forall \tilde{q} \in Q_H,
\end{aligned} \tag{11}$$

subject to the boundary condition $p_H = g$.

Remark 1. *The design of a "good" eigenvalue problem is a key ingredient of the GMsFEM. It plays a critical role in reducing the dimension of the coarse solution space. After applying such eigenvalue problem, a few dominant modes are selected to capture the multiscale behavior of the multiscale solution up to some certain extent.*

Remark 2. *Generally, the offline space should contain a constant basis function. Therefore, the local snapshot space $V_{snap}^{v,i}$, as a solution space of the eigenvalue Problem (9), can be decomposed into $V_1^{v,i} \bigoplus V_2^{v,i}$, where $V_1^{v,i} = \{(1, 1, \cdots, 1)\}$ and $V_2^{v,i} = \{\psi : \int_{E_i} \psi \cdot n_i = 0, \psi \in V_{snap}^{v,i}\}$. We note that the element with $\{(1, 1, \cdots, 1)\}$ in the snapshot space corresponds to the local solution with the unit normal flux on the edge and the elements of $V_2^{v,i}$ have average zero normal flux traces. We eliminate the constant boundary condition basis function in the snapshot space and put it, $(1, 1, \cdots, 1) \in V_1^{v,i}$, as the first basis function of the offline space, and identify the other dominant modes in the space $V_2^{v,i}$.*

3.2. Multiscale Solution Space V_H^q

We construct the solution space V_H^q and the testing space W_H^q for q_H. They follow a similar procedure to the one for v_H. In order to build V_H^q, the snapshot space V_{snap}^q is to be constructed. We define a local problem corresponding to each coarse-grid edge $E_i \in \mathcal{E}^H$ as follows: Find $(c_j^i, \psi_{q,j}^i) \in Q_h \times V_h^q$, such that

$$
\begin{aligned}
\psi_{q,j}^i + D\nabla c_j^i - v_H c_j^i &= 0 &&\text{in } K, \\
\nabla \cdot \psi_{q,j}^i &= \alpha_j^i &&\text{in } K, \\
\psi_{q,j}^i \cdot n &= 0 &&\text{on } \partial K \backslash E_i, \\
\psi_{q,j}^i \cdot n &= \delta_j^i &&\text{on } E_i,
\end{aligned}
\tag{12}
$$

where $K = K_r$ or K_s depicted in Figure 2. The local snapshot space $V_{snap}^{q,i}$, the snapshot space V_{snap}^q, and the snapshot matrix R_{snap}^q are formed as

$$
V_{snap}^{q,i} = \text{span}\{\psi_{q,j}^i : 1 \le j \le J_i\},
$$

$$
V_{snap}^q = \bigcup_{E_i} V_{snap}^{q,i} = \text{span}\{\psi_{q,j}^i : 1 \le j \le J_i, \ 1 \le i \le N_e\}.
\tag{13}
$$

$$
R_{snap}^q = \left[\psi_1^q, \psi_2^q, \cdots, \psi_{L_{snap}}^q\right],
$$

respectively.

To construct the testing space W_H^q, a snapshot space W_{snap}^q is also needed. We solve the adjoint problem of (12)

$$
\begin{aligned}
w_{q,j}^i - D\nabla p_j^i &= 0 &&\text{in } K, \\
\nabla \cdot w_{q,j}^i + \frac{1}{D}v_H \cdot w_{q,j}^i &= \alpha_j^i &&\text{in } K, \\
w_{q,j}^i \cdot n &= 0 &&\text{on } K \backslash E_i, \\
w_{q,j}^i \cdot n &= \delta_j^i &&\text{on } E_i.
\end{aligned}
\tag{14}
$$

Then, the snapshot space W_{snap}^q is formed by the snapshot functions $\omega_{q,j}^i$ for all $E_i \in \mathcal{T}^H$.

The local offline space $V_{\text{off}}^{q,i}$ for u_H is obtained by solving the following eigenvalue problem in $V_{\text{snap}}^{q,i}$:

$$A_q^{\text{off}} \Psi_k^q = \lambda_k M_q^{\text{off}} \Psi_k^q, \tag{15}$$

where

$$A_q^{\text{off}} = [a_{st}] = \int_{E_i} (\psi_{q,s}^i \cdot n)(\psi_{q,t}^i \cdot n),$$

and

$$M_q^{\text{off}} = [m_{st}] = \int_{\omega_i} \tilde{D} \psi_{q,s}^i \cdot \psi_{q,t}^i.$$

Here, we let $\tilde{D} = \frac{1+|v_H|}{D}$, where $|v_H|$ denotes the vector l^2 norm of v_H. Then, the local offline space $V_{\text{off}}^{q,i}$, the offline space V_{off}^q, and the offline matrix R_{off}^q are formed as:

$$V_{\text{off}}^{q,i} = \text{span}\{\phi_{q,k}^i : 1 \leq k \leq L_{\text{off}}^i\},$$

$$V_{\text{off}}^q = \bigcup_{E_i} V_{\text{off}}^{q,i} = \text{span}\{\phi_{q,k}^i : 1 \leq k \leq L_{\text{off}}^i, 1 \leq i \leq N_e\}, \tag{16}$$

$$R_{\text{off}}^q = \left[\phi_1^q, \phi_2^q, \cdots, \phi_{L_{\text{off}}}^q\right],$$

respectively. Here $\phi_{q,k}^i = \sum_{j=1}^{J_i} \Psi_{kj}^q \psi_{q,j}^i$, $k = 1, 2, \cdots, L_{\text{off}}^i$, is the dominant mode in the space $V_{\text{snap}}^{q,i}$.

We let $V_H^q = V_{\text{off}}^q$ and define the testing space as

$$W_H^q = \{w \in W_{\text{snap}}^q : (w - q) \cdot n|_E = 0, \text{ for all } E \in \mathcal{E}^H, \text{ for some } q \in V_H^q\}, \tag{17}$$

where n is the unit-normal vector of the coarse-grid edge E. Now, we have the multiscale solution space V_H^q and the testing space W_H^q. The GMsFEM solution (c_H, q_H) can be computed through (6).

Remark 3. *We remark that the fine-scale velocity field is constructed and used in computing multiscale basis functions for the concentration. In future, we plan to study joint multiscale basis construction procedures, which can compute multiscale basis functions for the concentration without solving the velocity field. Because the concentration field is a nonlinear function of the velocity field, an online procedure for computing multiscale basis functions for the concentration will be employed.*

4. Numerical Results

We present a representative set of numerical experiments that demonstrate the performance of the mixed GMsFEM for approximating the coupled flow and transport Equation (2). The computational domain $\Omega = [0,1] \times [0,1]$. We consider two different permeability fields κ, as depicted in Figures 3a,b. The source term f_c to be used are plotted in Figures 3c,d, and f_q is chosen to be 0. In all experiments below, the fine grid $\mathcal{T}^h$ is fixed to be 200×200 uniform mesh, *i.e.*, $h = 1/200$. The coarse grid consists of 20×20 uniform meshes, *i.e.*, $H = 1/20$. As for the time discretization, the time step is chosen to be $\tau = 1 \times 10^{-4}$ and the Crank-Nicolson scheme is used. We denote $\overline{c_h}$ as the average value of c_h in each coarse cell, *i.e.*, $\overline{c_h} = \frac{1}{|K|} \int_K c_h$, for every $K \in \mathcal{T}^H$. The relative numerical errors are measured in L^2 norm for the concentration.

(a) κ_1 in $\log_{10}$ scale

(b) κ_2 in $\log_{10}$ scale

(c) f_1

(d) f_2
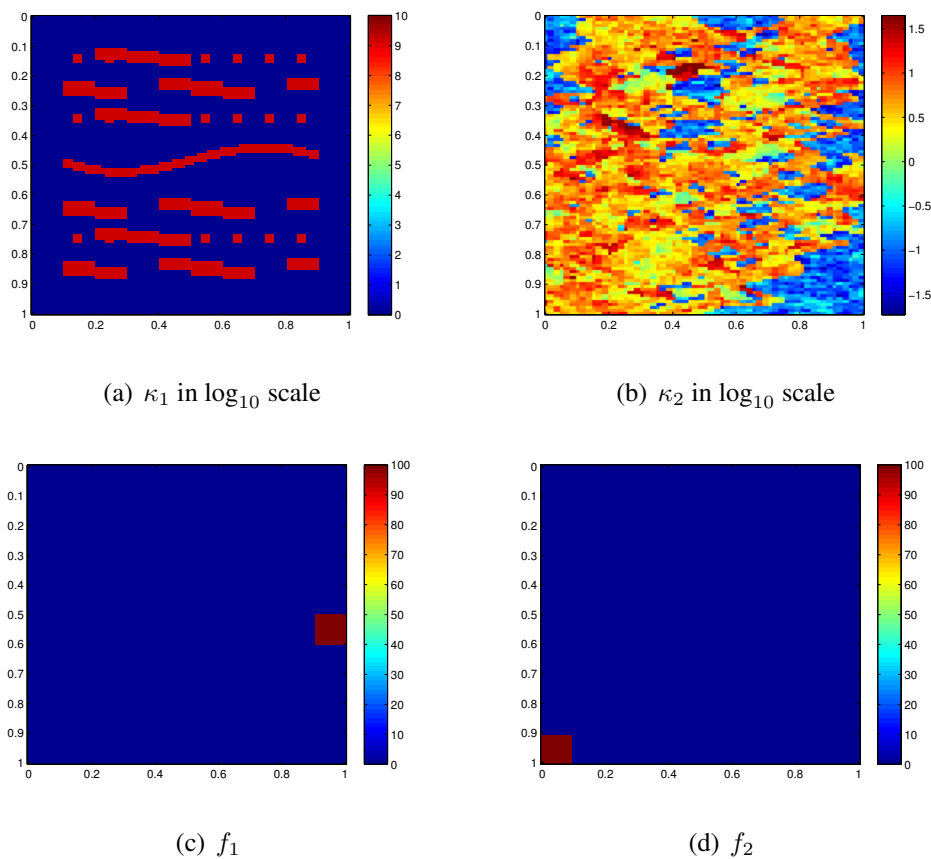
Figure 3. Two permeability fields (**a,b**) and two source terms (**c,d**).

In our numerical experiments, we approximate the velocity v_H and the flux q_H (at any time instant) in the offline space V_H^v and V_H^q in which each coarse edge is equipped with L_{off}^i basis functions. We choose at most $L_{\text{off}}^i = 2$ and compare concentration profiles with $L_{\text{off}}^i = 1$. Note that there are H/h basis functions associated with each coarse edge. We only select up to the two dominant modes per edge to form the offline space.

The first experiment is for the Problem (2), where the diffusivity $D = 1$, the source term $f_c = f_1$, the permeability field $\kappa = \kappa_1$, and the boundary condition $g = 7xy$. The boundary condition represents the flow from lower left corner to upper right corner. The Peclet number in the entire domain is 180.18, while the coarse-grid Peclet numbers vary with the maximum one being 11.01. In Figure 4, we depict the averaged fine-scale solutions and the GMsFEM solutions at the time $T = 0.015$, 0.04, and 0.1. We choose the averaged fine-scale solution since piecewise constant basis functions are used in the approximation of the concentration on a coarse grid. The averaged fine-scale solution is depicted on the top of Figure 4. In the middle row, we depict the GMsFEM solution, where only one basis function per edge is used for the approximation of the velocity and one basis function is used for the approximation of the flux-concentration field. The L^2 errors in the concentration field are 21.22%, 30.16%, and 27.19% at $T = 0.015$, 0.04, and 0.1. At the bottom row of Figure 4, we depict the concentrations computed using two basis functions for the velocity and two basis functions for the flux-concentration field. As we observe, the results look much better when two basis functions are used. For example, at $T = 0.1$, we can observe that the concentration profile is similar to the averaged fine-scale concentration profile.

The L^2 errors in the concentration field are 8.1%, 11.1%, and 8.44% at $T = 0.015$, 0.04, and 0.1. Note that since we use 20×20 coarse grid and piecewise constant basis functions for the concentration, one expects a first order convergence with respect to the coarse mesh (*i.e.*, about 5% error in our case).
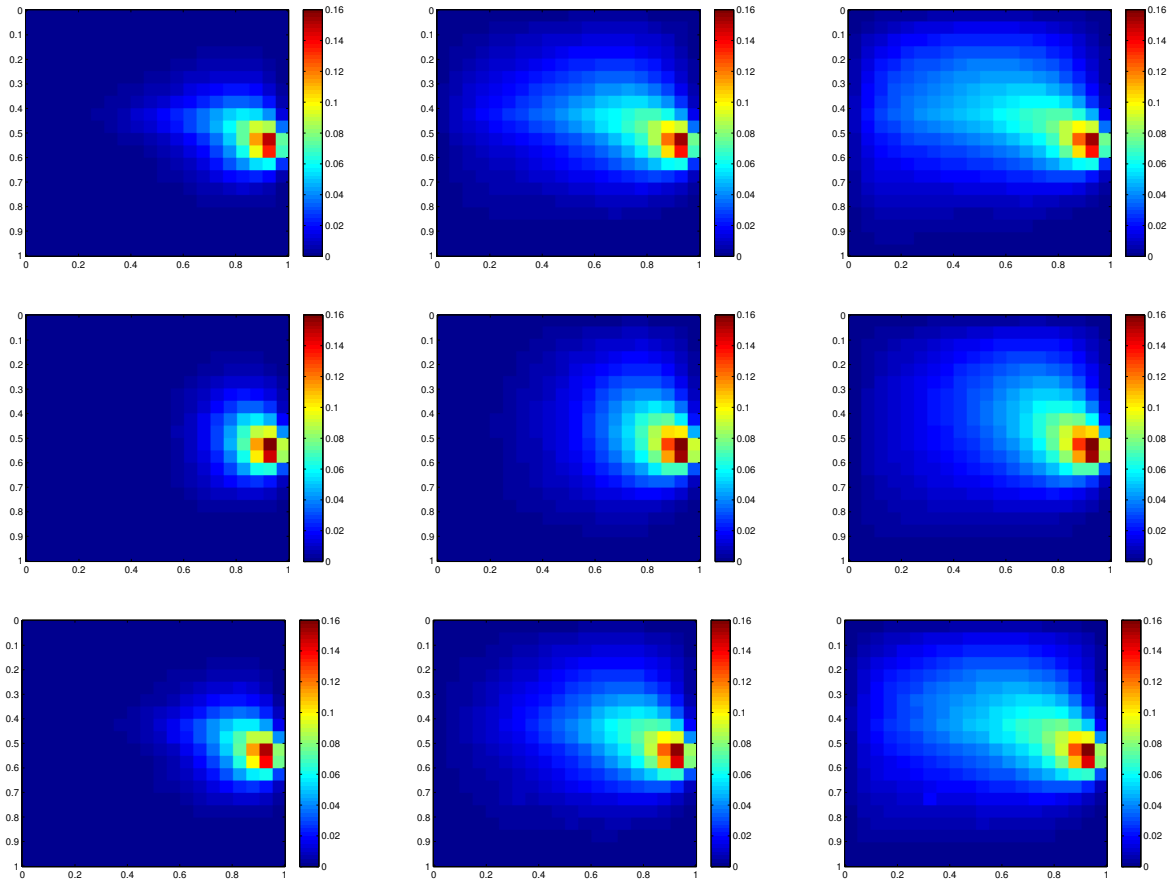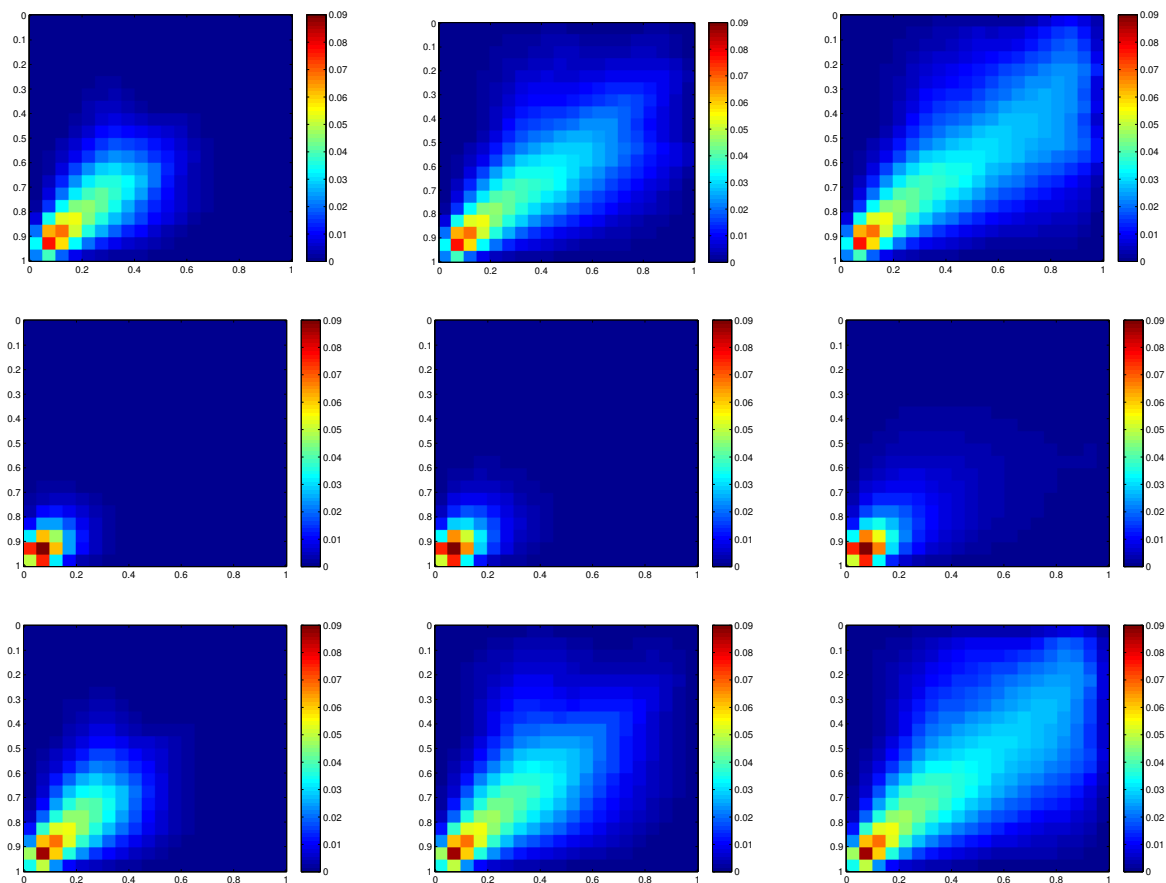

Figure 4. First row: Fine-scale solutions $\overline{c_h}$. Second row: GMsFEM solutions c_H (one multiscale basis function per edge for both velocity and flux-concentration). Third row: GMsFEM solutions c_H (two multiscale basis function per edge for both velocity and flux-concentration). From left column to right column: $T = 0.015$, 0.04, 0.1. We use $\kappa = \kappa_1$, $f_c = f_1$, H = 1/20.

In our second set of numerical examples, we consider the permeability $\kappa = \kappa_2$, a source term $f_c = f_2$, and a boundary condition $g = 8(x - y)$. We let the diffusivity to be $D = 1$. In this case, the problem becomes convection-dominated, where the coarse-grid Peclet number has a maximum value around 8.1. The numerical results are shown in Figure 5, where the top row shows the averaged fine-scale concentration profiles, the middle row shows the GMsFEM solution with one velocity basis per edge and one flux-concentration basis function, and the bottom row shows the GMsFEM solution, which uses two velocity basis functions and two flux-concentration basis functions. In all numerical results, we use piecewise constant pressure and piecewise constant concentration basis functions, as mentioned earlier. Thus, for the concentration field, there is an irreducible error of order H (5% in our case). First, we study the numerical results using only one multiscale basis function (the middle row of Figure 5). The L^2 errors in the concentration field are 77.6%, 82.53%, and 77.96% at $T = 0.01$, 0.02, and 0.1. We observe from

the figure that the results with one basis function per edge do not capture the averaged fine-scale solution behavior correctly. On the other hand, we observe a good agreement when two multiscale basis functions are used (the bottom row of Figure 5). We observe that the main features of the concentration profile are captured. The L^2 errors in the concentration field are 14.9%, 18.24%, and 15.71% at $T = 0.01$, 0.02, and 0.1.

In our numerical simulations, we limit ourselves to piecewise constant (lowest order) concentration basis functions. This allows a low computational cost and avoids a design of more complex concentration basis functions, which can satisfy inf-sup conditions (see e.g., [32]). Since we use lowest order basis functions for the concentration, the accuracy is limited to $O(H)$. This is reasonable as in large-scale simulations (due to very detailed κ), the coarse grid sizes can be taken sufficiently small. In general, the numerical results shown above can be improved using more basis functions for the flux-concentration and designing multiscale basis functions for the concentration field. One of our main objectives is to show that the results with one basis function per edge (which is similar to flow-based upscaling) can be substantially improved if one uses more multiscale basis functions, and we also provide a procedure for computing the multiscale basis functions and suitable global formulations.

Figure 5. First row: Fine-scale solutions $\overline{c_h}$. Second row: GMsFEM solutions c_H (one multiscale basis function per edge for both velocity and flux-concentration). Third row: GMsFEM solutions c_H (two multiscale basis function per edge for both velocity and flux-concentration). From left column to right column: $T = 0.01$, 0.02, 0.1. We use $\kappa = \kappa_2$, $f_c = f_2$, H = 1/20.

5. Discussions on Time Dependent Velocity

In our examples above, the velocity field was time-independent, and thus, the coupling between the flow and transport is weak. In above examples, we derived a multiscale coupling framework and demonstrated a robust framework for multiscale convection-diffusion equation. When the velocity field becomes time-dependent, one needs to re-calculate multiscale basis functions as velocity varies. There are several procedures, which we will mention, after a brief discussion on time varying velocity field scenarios. First, we remark on several scenarios, when the velocity field can depend on time (we call it "time-dependent" in our further discussions, even though the time may enter implicitly). The velocity field can depend on time via time-varying concentration field as in miscible or immiscible flows (e.g., [33] and the referenes therein) or the velocity field can, in addition, have a time-dependent component due to compressibility. We plan to address these application problems in our future works.

Computations of multiscale basis functions for the time-dependent velocity field can be performed offline [16,34] or using the residuals in the online stage [12,13]. For the offline computations, one needs a richer class of snapshot vectors, which can span possible velocity fields and perform the same local spectral decompositions and global coupling framework, as we discussed above. "Rich" snapshot spaces are discussed in [16] for parameter-dependent problem (the time can be treated as a parameter). Another approach for identifying multiscale basis functions, when the snapshot space is very large, is the use of l_1-minimization techniques as proposed in [34]. All these approaches can be used adaptively in space and time. Finally, one can use residual-based online basis functions [12,13], where one additional multiscale basis function is computed adaptively using the residual information. The success of these approaches depends on the offline space as it is shown, thus a good offline space is needed to achieve a high accuracy.

In some time-dependent velocity cases, one can get a good accuracy without modifying multiscale basis functions. For simplicity, we consider a "miscible" type flow and transport, which are described by

$$
\begin{aligned}
\frac{\partial c}{\partial t} + v \cdot \nabla c - D\Delta c &= f_c \quad \text{in } \Omega \times (0, T), \\
v + \zeta(c)\kappa\nabla p &= 0 \quad \text{in } \Omega, \\
\nabla \cdot v &= f_q \quad \text{in } \Omega.
\end{aligned}
\tag{18}
$$

We take $\zeta(c) = (c^2 + 0.2(1 - c)^2)$. We use the same setup as in the first example. The source term is the same, that is, $f_c = f_1$ and the boundary condition is $g = 28xy$. The numerical results are shown in Figure 6. The first row shows the averaged fine-scale concentration profiles and the second row shows the GMsFEM solution with two velocity basis and two flux-concentration basis functions. The L^2 errors in the concentration field are 5.81%, 8.63%, and 7.72% at $T = 0.015, 0.04$, and 0.1, respectively. These errors are comparable to the case with time-independent velocity field. We note that the errors are close to the irreducible error due to the coarse-mesh size.
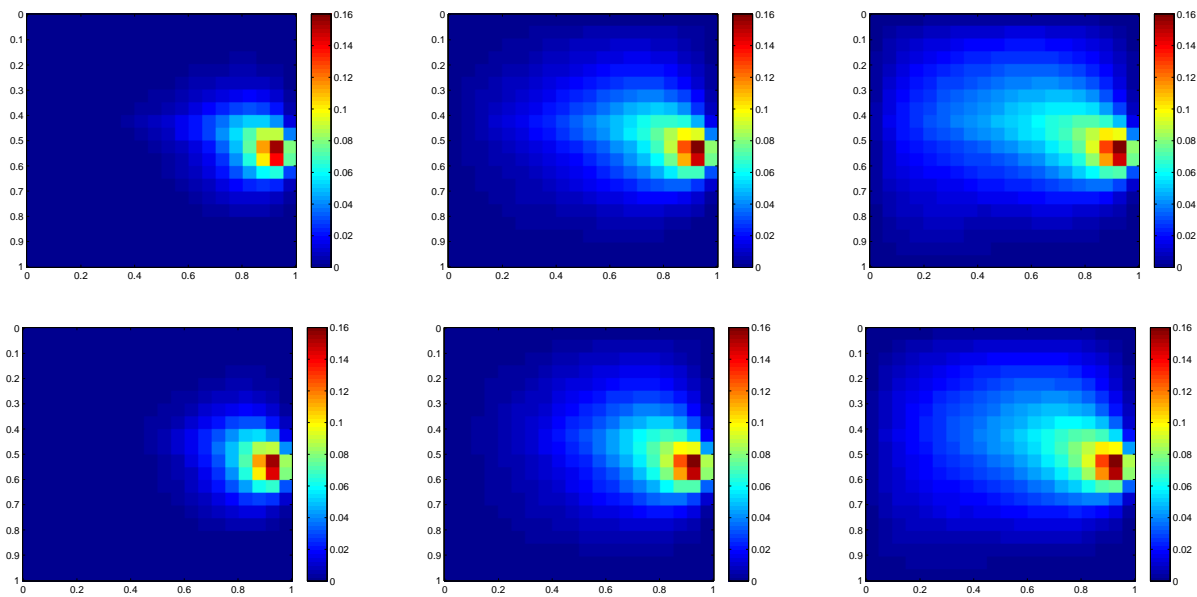
Figure 6. First row: Fine-scale solutions $\overline{c_h}$. Second row: GMsFEM solutions c_H (two multiscale basis function per edge for both velocity and flux-concentration). From left column to right column: $T = 0.015,\ 0.04,\ 0.1$. We use $\kappa = (c^2 + 0.2(1-c)^2)\kappa_1$, $f_c = f_1$, $H = 1/20$. Time-dependent velocity case.

6. Conclusions

In this paper, we develop a Generalized Multiscale Finite Element Method (GMsFEM) for coupled flow and transport equations. The transport equation is convection dominated and we choose an appropriate test space to achieve a stability and improve numerical results. We study a mixed formulation for both flow and transport, which guarantees mass conservation. The multiscale spaces for the flux and the velocity fields are constructed by appropriately choosing the snapshot spaces and performing local spectral decompositions. The design of the local test and trial multiscale spaces is one of our novel contributions. From the numerical experiments, we observe that one needs to have more than one multiscale basis function to capture the concentration profile on the coarse grid. In particular, using only two multiscale basis functions for the pressure equation and two multiscale basis functions for the concentration equation, we can achieve good accuracy. Our future studies will include a systematic design of multiscale basis functions for the concentration that can provide a stable discretization.

Author Contributions

Jun Ren was a lead in the paper. Wing Tat Leung, Eric T. Chung, Yalchin Efendiev contributed to the computations and method developments.

Conflicts of Interest

The authors declare no conflict of interest.

References

1. Chen, Y.; Durlofsky, L. An Ensemble Level Upscaling Approach for eFficient Estimation of fIne-Scale Production Statistics Using Coarse-Scale Simulations. In *SPE Reservoir Simulation Symposium*; Society of Petroleum Engineers: Houston, TX, USA, 2007.
2. Chen, Y.; Durlofsky, L.; Gerritsen, M.; Wen, X. A coupled local-global upscaling approach for simulating flow in highly heterogeneous formations. *Adv. Water Resour.* **2003**, *26*, 1041–1060.
3. Durlofsky, L.J. Numerical calculation of equivalent grid block permeability tensors for heterogeneous porous media. *Water Resour. Res.* **1991**, *27*, 699–708.
4. Aarnes, J.E.; Krogstad, S.; Lie, K.-A. A hierarchical multiscale method for two-phase flow based upon mixed finite elements and nonuniform grids. *Multiscale Model. Simul.* **2006**, *5*, 337–363.
5. Arbogast, T.; Pencheva, G.; Wheeler, M.F.; Yotov, I. A multiscale mortar mixed finite element method. *Multiscale Model. Simul.* **2007**, *6*, 319–346.
6. Brown, D.L.; Peterseim, D. A multiscale method for porous microstructures. *ArXiv E-Prints* **2014**, arXiv:1411.1944.
7. Bush, L.; Ginting, V.; Presho, M. Application of a conservative, generalized multiscale finite element method to flow models. *J. Comput. Appl. Math.* **2014**, *260*, 395–409.
8. Chan, H.Y.; Chung, E.T.; Efendiev, Y. Adaptive mixed gmsfem for flows in heterogeneous media. *ArXiv E-Prints* **2015**, arXiv:1507.01659.
9. Chung, E.; Efendiev, Y. Reduced-contrast approximations for high-contrast multiscale flow problems. *Multiscale Model. Simul.* **2010**, *8*, 1128–1153.
10. Chung, E.; Leung, W.T. A sub-grid structure enhanced discontinuous galerkin method for multiscale diffusion and convection-diffusion problems. *Comput. Phys.* **2013**, *14*, 370–392.
11. Chung, E.T.; Efendiev, Y.; Fu, S. Generalized multiscale finite element method for elasticity equations. *GEM-Int. J. Geomath.* **2014**, *5*, 225–254.
12. Chung, E.T.; Efendiev, Y.; Leung, W.T. An online generalized multiscale discontinuous galerkin method (gmsdgm) for flows in heterogeneous media. *ArXiv E-Prints* **2015**, arXiv:1504.04417.
13. Chung, E.T.; Efendiev, Y.; Leung, W.T. Residual-driven online generalized multiscale finite element methods. *ArXiv E-Prints* **2015**, arXiv:1501.04565.
14. Chung, E.T.; Efendiev, Y.; Li, G.; Vasilyeva, M. Generalized multiscale finite element methods for problems in perforated heterogeneous domains. *Appl. Anal.* **2015**, in press.

15. Chung, E.T.; Efendiev, Y.; Li, G. An adaptive GMsFEM for high-contrast flow problems. *J. Comput. Phys.* **2014**, *273*, 54–76.

16. Efendiev, Y.; Galvis, J.; Hou, T. Generalized multiscale finite element methods. *J. Comput. Phys.* **2013**, *251*, 116–135.

17. Efendiev, Y.; Galvis, J.; Lazarov, R.; Willems, J. Robust domain decomposition preconditioners for abstract symmetric positive definite bilinear forms. *ESAIM Math. Model. Numer. Anal.* **2012**, *46*, 1175–1199.

18. Efendiev, Y.; Galvis, J.; Vassilevski, P.S. Spectral Element Agglomerate Algebraic Multigrid Methods for Elliptic Problems with High-Contrast Coefficients. In *Domain Decomposition Methods in Science and Engineering XIX*; Springer: Heidelberg, Germany, 2011.

19. Efendiev, Y.; Hou, T.; Wu, X.H. Convergence of a nonconforming multiscale finite element method. *SIAM J. Numer. Anal.* **2000**, *37*, 888–910.

20. Hajibeygi, H.; Kavounis, D.; Jenny, P. A hierarchical fracture model for the iterative multiscale finite volume method. *J. Comput. Phys.* **2011**, *230*, 8729–8743.

21. Henning P.; Peterseim, D. Oversampling for the multiscale finite element method. *Multiscale Model. Simul.* **2013**, *11*, 1149–1175.

22. Hou, T.; Wu, X.H. A multiscale finite element method for elliptic problems in composite materials and porous media. *J. Comput. Phys.* **1997**, *134*, 169–189.

23. Jenny, P.; Lee, S.H.; Tchelepi, H. Multi-scale finite volume method for elliptic problems in subsurface flow simulation. *J. Comput. Phys.* **2003**, *187*, 47–67.

24. Kaulmann, S.; Flemisch, B.; Haasdonk, B.; Lie, K.A.; Ohlberger, M. The localized reduced basis multiscale method for two-phase flows in porous media. *Int. J. Numer. Methods Eng.* **2015**, *102*, 1018–1040.

25. Målqvist, A.; Peterseim, D. Localization of elliptic multiscale problems. *Math. Comput.* **2014**, *83*, 2583–2603.

26. Presho, M.; Galvis, J. A mass conservative generalized multiscale finite element method applied to two-phase flow in heterogeneous porous media. *ArXiv E-Prints* **2015**, arXiv:1504.02033.

27. Arbogast, T.; Wheeler, M.F.; Yotov, I. Mixed finite elements for elliptic problems with tensor coefficients as cell-centered finite differences. *SIAM J. Numer. Anal.* **1997**, *34*, 828–852.

28. Douglas Jr, J.; Ewing, R.E.; Wheeler, M.F. The approximation of the pressure by a mixed method in the simulation of miscible displacement. *RAIRO-Anal. Numérique* **1983**, *17*, 17–33.

29. Durlofsky, L.J. A triangle based mixed finite element-finite volume technique for modeling two phase flow through porous media. *J. Comput. Phys.* **1993**, *105*, 252–266.

30. Ewing, R.E.; Russell, T.F.; Wheeler, M.F. Convergence analysis of an approximation of miscible displacement in porous media by mixed finite elements and a modified method of characteristics. *Comput. Methods Appl. Mech. Eng.* **1984**, *47*, 73–92.

31. Calo, V.M.; Chung, E.T.; Efendiev, Y.; Leung, W.T. Multiscale stabilization for convection-dominated diffusion in heterogeneous media. *ArXiv E-Prints* **2015**, arXiv:1509.06833.

32. Chung, E.T.; Efendiev, Y.; Lee, C.S. Mixed generalized multiscale finite element methods and applications. *Multiscale Model. Simul.* **2015**, *13*, 338–366.

33. Ewing, R.; Efendiev, Y.; Ginting, V.; Wang, H. *Upscaling of Transport Equations for Multiphase and Multicomponent Flows*; Springer: Heidelberg, Germany, 2008.

34. Chung, E.; Efendiev, Y.; Leung, T.W.; Li, G. Sparse generalized multiscale finite element methods and their applications. *ArXiv E-Prints* **2015**, arXiv:1506.08509.